Micro-bubbles and Micro-particles are Not Faithful Tracers of Turbulent Acceleration

Varghese Mathai,[1] Enrico Calzavarini,[2,*] Jon Brons,[1,3] Chao Sun,[4,1,†] and Detlef Lohse[1,5]

[1] *Physics of Fluids Group, Faculty of Science and Technology, Mesa+ Institute, University of Twente, 7500 AE Enschede, The Netherlands.*
[2] *Univ. Lille, CNRS, FRE 3723, LML, Laboratoire de Mecanique de Lille, F 59000 Lille, France*
[3] *Applied Mathematics Research Centre, Faculty of Engineering and Computing, Coventry University, Priory Street, Coventry CV1 5FB, United Kingdom.*
[4] *Center for Combustion Energy and Department of Thermal Engineering, Tsinghua University, 100084 Beijing, China.*
[5] *Max Planck Institute for Dynamics and Self-Organization, 37077 Göttingen, Germany.*

(Dated: June 17, 2016)

EXPERIMENTAL SETUP

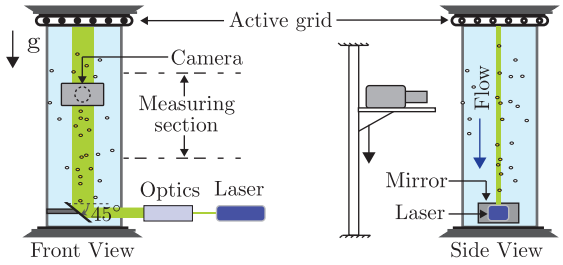

FIG. 1: Schematic of the measurement section of the Twente Water Tunnel. Bubbles and neutrally buoyant tracer particles of diameters $\approx$ 150 $\pm$ 25 μm and $\approx$ 125 μm, respectively, were dispersed in the flow for particle tracking experiments.

PARTICLE EQUATION OF MOTION

The model equation of motion for a small inertial spherical particle advected by a fluid flow field, with velocity $\mathbf{U}(\mathbf{X}(\mathcal{T}),\mathcal{T})$, is:

$$\mathcal{V}\ \rho_p\ \ddot{\mathbf{X}} = \mathcal{V}\ \rho_f \frac{D\mathbf{U}}{D\mathcal{T}} + \mathbf{F_{AM}} + \mathbf{F_D} + \mathbf{F_B} \qquad (1)$$

where $\mathcal{V} = \frac{4}{3}\pi a^3$ is the particle volume, with a being the particle radius, and ρ_f and ρ_p the fluid and particle mass densities, respectively. The forces contributing on the right-hand-side besides the fluid acceleration (which includes the pressure gradient term) are the added mass $\mathbf{F_{AM}}$, the drag force $\mathbf{F_D}$, and the buoyancy $\mathbf{F_B}$ [1–3]:

$$\mathbf{F_{AM}} = \mathcal{V}\ \rho_f C_M \left(\frac{D\mathbf{U}}{D\mathcal{T}} - \ddot{\mathbf{X}}\right), \qquad (2)$$

$$\mathbf{F_D} = 6\ \pi\ \mu\ a\ (\mathbf{U} - \dot{\mathbf{X}}), \qquad (3)$$

$$\mathbf{F_B} = \mathcal{V}\ (\rho_p - \rho_f)\ g\ \hat{\mathbf{e}}_z, \qquad (4)$$

where μ is the dynamic viscosity, g is the gravity intensity and $\hat{\mathbf{e}}_z$ is the unit-vector in the direction of gravity. Note that we use the inviscid added mass coefficient for a sphere, i.e $C_M = 1/2$. This leads to

$$\ddot{\mathbf{X}} = \frac{3\rho_f}{\rho_f + 2\rho_p}\left(\frac{D\mathbf{U}}{D\mathcal{T}} + \frac{12\nu}{d_p^2}(\mathbf{U} - \dot{\mathbf{X}}) + g\ \hat{\mathbf{e}}_z\right) - g\ \hat{\mathbf{e}}_z, \qquad (5)$$

where $\nu \equiv \mu/\rho_f$ is the kinematic viscosity, and d_p is the particle diameter. Here we neglect lift, history, and finite-size Faxén forces, since these are verified to be small in point-particle limit and when the particle size is smaller than the Kolmogorov length scale η of the flow [4–6].

FROUDE NUMBER EFFECT

We first consider the effect of changing the ratio of turbulent to gravitational acceleration, i.e a_η/g, which, according to [7], equals the Froude number. Gravity enhances the acceleration in both vertical and horizontal directions (Fig. 2). The vertical acceleration is consistently lower compared to the horizontal, in agreement with our experiments. This is accompanied by a decrease in correlation time (Fig. 3), as also evidenced by our experiments.

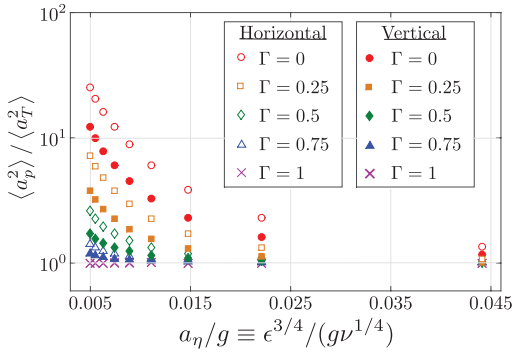

FIG. 2: Normalized acceleration variance for buoyant particles vs a_η/g obtained from Eulerian-Lagrangian DNS at $\mathrm{Re}_\lambda \approx 80$. Hollow and solid symbols correspond to horizontal and vertical components, respectively.

NON-DIMENSIONALIZATION

When the advecting flow is turbulent and the particle spatial extension is of the order of the dissipative scale of turbulence, it is appropriate to non-dimensionalize eq. (5) with respect to the Kolmogorov units: η (length) and τ_η (time). This leads to

$$\ddot{\mathbf{x}} = \beta \frac{D\mathbf{u}}{Dt} + \frac{1}{\mathrm{St}}(\mathbf{u} - \dot{\mathbf{x}}) + \frac{1}{\mathrm{Fr}}\hat{\mathbf{e}}_z, \tag{6}$$

where small case letters denote the new dimensionless variables and the following control parameters have been defined:

$$\beta \equiv \frac{3\rho_f}{\rho_f + 2\rho_p}; \quad \mathrm{St} \equiv \frac{d_p^2}{12\beta\nu\tau_\eta} = \frac{\tau_p}{\tau_\eta}; \quad \mathrm{Fr} \equiv \frac{a_\eta}{(\beta - 1)\, g} \tag{7}$$

Note that the Stokes number St is defined taking added mass into account, and the Froude number Fr is a modified one that takes the particle density, through β, into account. Therefore these definitions are valid for a particle of arbitrary density.

In the high turbulence intensity limit ($\mathrm{Fr} \to \infty$), the third right-hand-side term in the equation of motion can be neglected. Under this condition the vanishing St limit leads to $\dot{\mathbf{x}} \simeq \mathbf{u}$ for the velocity, and for the acceleration to $\ddot{\mathbf{x}} \simeq D_t\mathbf{u}$, where $D_t\mathbf{u}$ denotes the fluid-tracer acceleration.

At finite Fr, the small St limit leads to $\dot{\mathbf{x}} \simeq \mathbf{u} + \frac{\mathrm{St}}{\mathrm{Fr}}\hat{\mathbf{e}}_z$. For the particle acceleration this implies:

$$\ddot{\mathbf{x}} \simeq D_t\mathbf{u} + \frac{\mathrm{St}}{\mathrm{Fr}}\partial_z\mathbf{u} \tag{8}$$

ACCELERATION VARIANCE

We consider the single-component acceleration variance. These are

$$\langle \ddot{x}^2 \rangle \;\simeq\; \langle (D_t u_x)^2 \rangle + \left(\frac{\mathrm{St}}{\mathrm{Fr}}\right)^2 \langle (\partial_z u_x)^2 \rangle, \tag{9}$$

$$\tag{10}$$

where x and z are the horizontal and vertical components, respectively. Note that the linear terms in St/Fr vanish because there is no correlation between terms of the type $\mathbf{u}\cdot\nabla u_i$ and $\partial_z u_i$, i.e. there is no instantaneous correlation between the velocity field and its gradient.

Under isotropic turbulent conditions, the following relations are verified [8]:

$$\langle (\partial_Z U_X)^2 \rangle \simeq \frac{2}{15}\frac{\epsilon}{\nu}, \tag{11}$$

$$\langle (\partial_Z U_Z)^2 \rangle \simeq \frac{1}{15}\frac{\epsilon}{\nu}, \tag{12}$$

$$\langle (D_\mathcal{T} U_i)^2 \rangle = a_0 \epsilon^{3/2} \nu^{-1/2}, \tag{13}$$

where i denotes one of the components x, y, or z, and a_0 is the so-called Heisenberg-Yaglom constant. From this, one obtains the relations linking the acceleration variance of particles to that of fluid tracers

$$\frac{\langle \ddot{x}^2 \rangle}{\langle (D_t u_x)^2 \rangle} \;\simeq\; 1 + \frac{2}{15 a_0}\left(\frac{\mathrm{St}}{\mathrm{Fr}}\right)^2 \tag{14}$$

$$\frac{\langle \ddot{z}^2 \rangle}{\langle (D_t u_x)^2 \rangle} \;\simeq\; 1 + \frac{1}{15 a_0}\left(\frac{\mathrm{St}}{\mathrm{Fr}}\right)^2 \tag{15}$$

These predictions are applicable to both heavy ($\mathrm{St/Fr} < 1$) and light ($\mathrm{St/Fr} > 1$) particles of arbitrary density. On the experimental side, we have confirmed the enhancement of acceleration variance using tiny air-bubbles dispersed in our water tunnel facility. For heavy-particles, our predictions remain to be experimentally verified.

LAGRANGIAN TIME CORRELATION

In Fig. 3(a), we plot the simulation results for the evolution of Lagrangian time-correlation of acceleration with the ratio St/Fr. The left branch points to heavy particle, and the right one, to light particles. With increasing magnitude of St/Fr, we observe a decline in the correlation time for both heavy and light particles. Clearly, the drifting of the buoyant or heavy particle through the flow affects the correlation time. We model this by considering the case of a particle drifting through the flow at a speed u_r. In the absence of particle drift, it is well-known that the decorrelation time is $\tau_T \sim \tau_\eta$ [9]. Based on the characteristic velocity of a particle in the turbulent flow, u_{rms}, we estimate the length scale corresponding to this decorrelation time as $\Lambda \sim u_{rms}\tau_\eta$. Now, for a buoyant or heavy particle, the time of correlation is reduced due to an extra drift speed. Therefore, the new correlation time may be written as $\tau_p \approx \tau_T/(1 + u_r/u_{rms})$. For homogeneous isotropic turbulence the u_{rms} may be expressed in terms of the Re_λ and the u_η. This leaves us with the expression: $\tau_p/\tau_T \approx 1/(1 + \sqrt[4]{5/(3\mathrm{Re}_\lambda^2)}\frac{\mathrm{St}}{\mathrm{Fr}})$. The predictions, shown by the solid black curve, are in reasonable agreement with our numerical observations.

While the model provides reasonable predictions for the decorrelation time, we observe some small deviations from small to moderate St/Fr values in Fig. 3(a). Below, we provide an explanation for these deviations. From eq. (8), we note that the acceleration of a drifting particle has two contributions: (a) $D_t\mathbf{u}$ from the fluid tracer acceleration, and (b) $\frac{\mathrm{St}}{\mathrm{Fr}}\partial_z\mathbf{u}$ from the velocity-gradients in the flow. In Fig. 3(b)-(e), we show the normalized time correlation of the particle accelerations and the gradient terms along the particle trajectories. For small St/Fr, the velocity gradient terms ($\partial_z u_z$ and $\partial_z u_x$) decorrelate slower as compared to the fluid acceleration term (see

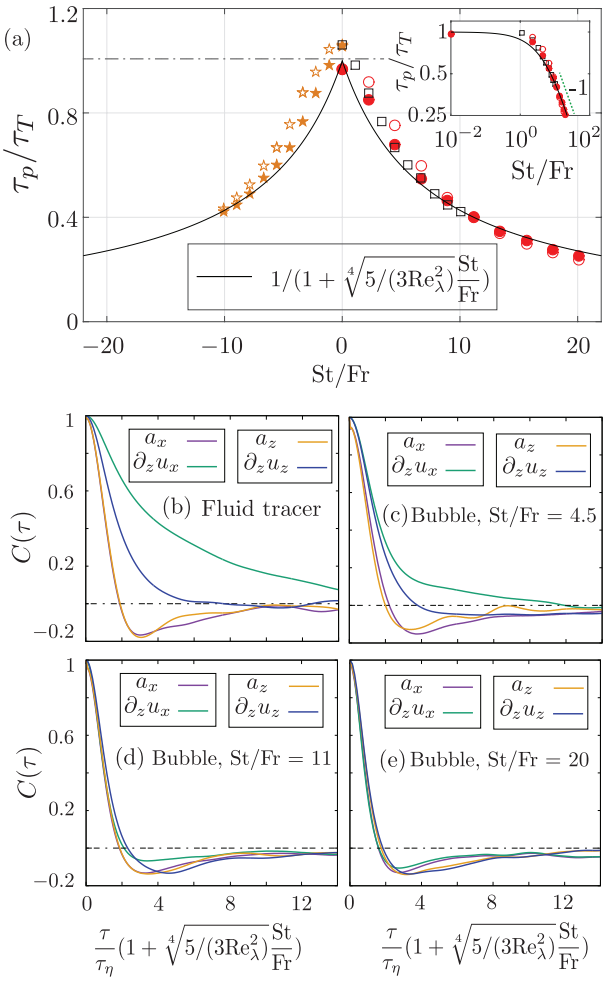

FIG. 3: (a) Normalized correlation time for bubbles ($\beta = 3$) and very heavy ($\beta = 0$) particles vs St/Fr obtained from Eulerian-Lagrangian DNS at $\mathrm{Re}_\lambda \approx 75$. The curve in black color shows the theoretical prediction, and the inset shows the plot on log-log scale. (b)-(e) Normalized autocorrelation function for fluid tracers and bubbles at different St/Fr values. Here, a_x and a_z are the horizontal and vertical accelerations, respectively. $\partial_z u_x$ and $\partial_z u_z$ are the spatial-velocitiy gradients, which contribute to the a_x and a_z, respectively. In (c)-(e) St/Fr increases from 4.5 to 20.

Fig. 3(b) & (c)). Since St/Fr is small, the fluid acceleration term $D_t\mathbf{u}$ dominates over the velocity gradient term $\frac{\mathrm{St}}{\mathrm{Fr}}\partial_z\mathbf{u}$. This explains the slower decrease in the decorrelation time in the numerics as compared to our predictions for small St/Fr (see |St/Fr|< 5 in Fig. 3(a)). Some additional observations may be made for the moderate St/Fr range. From Fig. 3(a), we note that the vertical component of particle acceleration (solid symbols) is shorter-correlated compared to the horizontal component (hollow symbols). This occurs because the fluid velocity gradient components are not all correlated in the same way. Due to the incompressibility constraint ($\partial_i u_i = 0$), the longitudinal gradient $\partial_z u_z$ is shorter-correlated compared to the transverse gradient $\partial_z u_x$, as may be seen in Fig. 3(b) & (c). Since the vertical acceleration is influenced by the longitudinal velocity-gradient, it decorrelates in shorter time than the horizontal acceleration. We now consider the case of large St/Fr in Fig. 3(a). In this case, the velocity gradient term $\frac{\mathrm{St}}{\mathrm{Fr}}\partial_z\mathbf{u}$ in eq. (8) dominates over the fluid acceleration term $D_t\mathbf{u}$, and therefore, the decrease in correlation time in DNS is in good agreement with the predictions of our eddy-crossing model.

ACCELERATION INTERMITTENCY

Intermittency, i.e. the observed strong deviations from Gaussianity, can be characterized in terms of the flatness of acceleration $\mathcal{F}(a_p) \equiv \langle a_p^4 \rangle / \langle a_p^2 \rangle^2$. Assuming statistical independence between $D_t u_i$ and $\partial_z u_i$[1], we obtain the tracer-normalized flatness of particle acceleration,

$$\frac{\mathcal{F}(\ddot{x})}{\mathcal{F}(D_t u_x)} = \frac{1 + \frac{12}{15\ a_0 \mathcal{F}(D_t u_x)} \left(\frac{\mathrm{St}}{\mathrm{Fr}}\right)^2 \left(1 + \frac{\mathcal{F}(\partial_z u_x)}{45\ a_0} \left(\frac{\mathrm{St}}{\mathrm{Fr}}\right)^2\right)}{1 + 2\frac{2}{15\ a_0}\left(\frac{\mathrm{St}}{\mathrm{Fr}}\right)^2 + \left(\frac{2}{15\ a_0}\right)^2 \left(\frac{\mathrm{St}}{\mathrm{Fr}}\right)^4} \tag{16}$$

$$\frac{\mathcal{F}(\ddot{z})}{\mathcal{F}(D_t u_x)} = \frac{1 + \frac{6}{15\ a_0 \mathcal{F}(D_t u_x)} \left(\frac{\mathrm{St}}{\mathrm{Fr}}\right)^2 \left(1 + \frac{\mathcal{F}(\partial_z u_z)}{90\ a_0} \left(\frac{\mathrm{St}}{\mathrm{Fr}}\right)^2\right)}{1 + 2\frac{1}{15\ a_0}\left(\frac{\mathrm{St}}{\mathrm{Fr}}\right)^2 + \left(\frac{1}{15\ a_0}\right)^2 \left(\frac{\mathrm{St}}{\mathrm{Fr}}\right)^4} \tag{17}$$

In the limit of small St/Fr,

$$\frac{\mathcal{F}(\ddot{x})}{\mathcal{F}(D_t u_x)} \simeq 1 - \frac{4}{15\ a_0}\left(1 - \frac{3}{\mathcal{F}(D_t u_x)}\right)\left(\frac{\mathrm{St}}{\mathrm{Fr}}\right)^2 \tag{18}$$

$$\frac{\mathcal{F}(\ddot{z})}{\mathcal{F}(D_t u_x)} \simeq 1 - \frac{2}{15\ a_0}\left(1 - \frac{3}{\mathcal{F}(D_t u_x)}\right)\left(\frac{\mathrm{St}}{\mathrm{Fr}}\right)^2 \tag{19}$$

It is verified that $\mathcal{F}(D_t u_x) > 3$. Therefore, both components are decreasing functions of St/Fr, with the vertical being larger than the horizontal one for small St/Fr.
In the large St/Fr limit,

$$\frac{\mathcal{F}(\ddot{x})}{\mathcal{F}(D_t u_x)} \simeq \frac{\mathcal{F}(\partial_z u_x)}{\mathcal{F}(D_t u_x)} \tag{20}$$

$$\frac{\mathcal{F}(\ddot{z})}{\mathcal{F}(D_t u_x)} \simeq \frac{\mathcal{F}(\partial_z u_z)}{\mathcal{F}(D_t u_x)} \tag{21}$$

It is verified that $\mathcal{F}(\partial_z u_z) < \mathcal{F}(\partial_z u_x) < \mathcal{F}(D_t u_x)$ [10]. This leads to the prediction $\mathcal{F}(a_v) < \mathcal{F}(a_h)$ i.e. vertical acceleration is less intermittent compared to the horizontal.

INTERPRETATION

Eq. (18)-(19) and eq. (20)-(21) provide predictions for the normalized acceleration flatness (intermittency) in the limits

[1] The absence of correlations between $D_t u_i$ and $\partial_z u_i$ is a first order (to be refined) approximation.

of small St/Fr and large St/Fr, respectively. Eq. (18)-(19) predict that the vertical component of flatness exceeds the horizontal one in the small St/Fr limit, while eq. (20)-(21) predict that the horizontal component exceeds the vertical one when St/Fr is large. Therefore, an interesting cross-over is predicted between the flatness factors of the two components as one moves from small St/Fr to large St/Fr. In Fig. 4, we present our numerical results in the small St/Fr range (St/Fr < 1). Despite the scatter in data, we make some interesting observation about our numerical results. With the exception of a single datapoint, the vertical components (solid symbols) are always higher compared to the horizontal components (hollow symbols), in agreement with eq. (18)-(19). In the large St/Fr limit, as was clear from Figure 4(c) of the main paper, the horizontal component exceeded the vertical one, again in agreement with our predictions (eq. (20)-(21)). Therefore, the cross-over predicted by us is qualitatively seen in our simulations as well. A quantitative agreement is missing since the higher moments (Flatness) are in general very sensitive. Moreover, the lowest Stokes numbers possible in simulations is ≈ 0.05, which is still an approximation of the St $\to 0$ limit. In addition, the predictions are subject to a few assumptions, such as the absence of correlation between velocity field and its gradient. While this is reasonable, it is not an exact result. At present, we do not have the resolution to verify the intricate details of (18)-(19). These aspects may be tested in future studies.

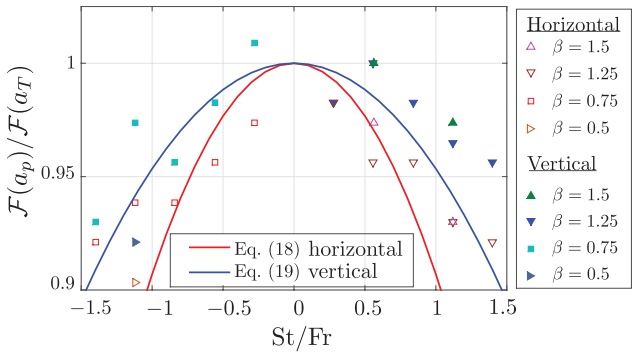

FIG. 4: Normalized Flatness factor in the small St/Fr limit. Hollow symbols show the flatness fo horizontal acceleration. Solid symbols show the flatness of vertical acceleration. The vertical acceleration flatness is mostly higher in numerics, in qualitative agreement with the predictions of eq. (18)-(19).

A GENERALIZED APPROACH

We discuss some of these recent analytical and numerical approaches for heavy particles. Interesting effects have been demonstrated on the gravity-induced modification of heavy particle statistics [7, 11–14], which were quantified as a function of particle inertia (St) and the Froude number given by the ratio of turbulent to gravitational acceleration (a_η/g). We examine the Stokes and Froude number definitions used in these studies. The Stokes number was defined as $\mathrm{St} \equiv \frac{\rho_p d_p^2}{18\rho_f \nu \tau_\eta}$ [7, 12, 14]. This definition is appropriate at large ρ_p/ρ_f, when added mass effects are negligible. We also note that the definition of Froude number as a_η/g [7, 14] does not take the particle density into account. Here, a_η is the turbulent acceleration and g is the gravitational acceleration. This Froude number definition is applicable when the particles under consideration are of fixed ρ_p/ρ_f. Therefore, these results apply to the case of very heavy particles and when the density ratio is kept constant, i.e $\rho_p/\rho_f = \text{constant} \gg 1$.

In this paper (main article), we provide a generalized description that is applicable to particles of arbitrary density. We have numerically shown the validity of our theoretical preditions for particles of arbitrary density. The theory we develop for isotropic turbulence can explain also our experimental findings on bubbles in a turbulent water flow. The generic St and Fr definitions we use converge to the definitions in [7, 12, 14] at large ρ_p/ρ_f. Therefore, such a modified approach may be useful for future studies that explore the effects of gravity for arbitrary-density particles in turbulence.

* enrico.calzavarini@polytech-lille.fr
† chaosun@tsinghua.edu.cn

[1] M. R. Maxey and J. J. Riley, Phys. Fluids **26**, 883 (1983).
[2] R. Gatignol, J. Mec. Theor. Appl. **2**, 143 (1983).
[3] P. Spelt and A. Biesheuvel, J. Fluid Mech. **336**, 221 (1997).
[4] E. Calzavarini, R. Volk, E. Leveque, J. F. Pinton, and F. Toschi, Physica (Amsterdam) **241D**, 237 (2012).
[5] E. Calzavarini, R. Volk, M. Bourgoin, E. Leveque, J. F. Pinton, and F. Toschi, J. Fluid Mech. **630**, 179 (2009).
[6] Y. Tagawa, J. M. Mercado, V. N. Prakash, E. Calzavarini, C. Sun, and D. Lohse, J. Fluid Mech. **693**, 201 (2012).
[7] J. Bec, H. Homann, and S. S. Ray, Phys. Rev. Lett. **112**, 184501 (2014).
[8] J. Hinze, *0. 1975 turbulence* (1972).
[9] P. Yeung and S. Pope, J. Fluid Mech. **207**, 531 (1989).
[10] T. Ishihara, Y. Kaneda, M. Yokokawa, K. Itakura, and A. Uno, J. Fluid Mech. **592**, 335 (2007).
[11] K. Gustavsson, S. Vajedi, and B. Mehlig, Phys. Rev. Lett. **112**, 214501 (2014).
[12] H. Parishani, O. Ayala, B. Rosa, L.-P. Wang, and W. Grabowski, Phys. Fluids **27**, 033304 (2015).
[13] A. Aliseda, A. Cartellier, F. Hainaux, and J. C. Lasheras, J. Fluid Mech. **468**, 77 (2002).
[14] P. J. Ireland, A. D. Bragg, and L. R. Collins, arXiv preprint arXiv:1507.07022 (2015).